



# Accelerated discovery of magnesium intermetallic compounds with sluggish corrosion cathodic reactions through active learning and DFT calculations

Yaowei Wang<sup>a</sup>, Qingli Tang<sup>a</sup>, Xinchen Xu<sup>b</sup>, Paul Weng<sup>a</sup>, Tao Ying<sup>b</sup>, Yao Yang<sup>b</sup>,  
Xiaoqin Zeng<sup>b,\*</sup>, Hong Zhu<sup>a,b,\*</sup>

<sup>a</sup> University of Michigan - Shanghai Jiao Tong University Joint Institute, Shanghai Jiao Tong University, Shanghai 200240, PR China

<sup>b</sup> State Key Laboratory of Metal Matrix Composites, Shanghai Jiao Tong University, Shanghai 200240, PR China

## ARTICLE INFO

### Keywords:

Magnesium alloys  
Intermetallic compounds  
Hydrogen evolution reaction  
First-principles calculation  
Active learning

## ABSTRACT

Magnesium (Mg) alloys can potentially be widely applied in transportation, aerospace and biomedical fields due to the light weight and biocompatibility. However, they are usually subjected to serious galvanic corrosions due to high chemical activity. In this work, active learning is employed to discover the intermetallic compounds which can suppress the corrosion cathodic reaction of Mg alloys. The hydrogen adsorption energy, which is a descriptor for the rate of the cathodic hydrogen evolution reaction (HER), is predicted by machine learning models using the geometric and chemical features of the H adatom's Voronoi neighbors. After five active learning iterations, the prediction error of the H adsorption energy for the strong/weak adsorption configuration is 0.196 eV (MAE) with the training set size less than 1% unknown data set. Furthermore, we find that the surfaces with strong H adsorption transfer more electrons to H adatoms than the weak H adsorption surfaces. Finally, the ability of the binary Mg intermetallics to inhibit the HER is ranked according to their surface stabilities and predicted H adsorption energies. This work suggests the binary Mg intermetallics that could greatly suppress the corrosion cathodic reaction through active learning and density functional theory (DFT) simulations, which is expected to accelerate the design of corrosion-resistant Mg alloys.

## 1. Introduction

The design of metal alloys with high strength, low weight and long service life is the crucial component in achieving carbon neutral [1]. Magnesium (Mg) alloys, as the lightest structural metals, are becoming more widely applied in automotive industry, medical applications and battery anodes [2–4]. The key to unlock the full potential of Mg is to control the fast corrosion rate due to its high reactivity [5]. Corrosion, which is the destructive attack of materials during their reaction with the environment, usually occurs through the operation of coupled electrochemical half-cell reactions [6]. For Mg alloys, the typical cathodic reaction is hydrogen evolution reaction (HER), which happens on intermetallics or noble impurities [7]. It should be noted that oxygen reduction reaction (ORR) has also gained attention in recent years. For example, Wang et al. [8] used spatially resolved localized techniques to explore the contribution of oxygen reduction reaction to Mg corrosion. Silva et al. measured both the oxygen concentration and local current

density on the proximate surface of Mg simultaneously [9] and found a correlation between the consumption of dissolved oxygen and cathodic activity. Wang et al. [10] observed a difference in polarization curve for the AZ31 under aerated and nonaerated conditions in various NaCl concentrations. However, except in high-purity Mg, the ORR is believed to contribute minimally to the cathodic corrosion reaction of most Mg alloys [8,11–13].

Some prior attempts to improve the corrosion resistance of Mg alloys include alloying, surface coating and dissolution modulators [14–19]. Among these attempts, alloying could improve corrosion performance and mechanical properties simultaneously by refining the microstructure or introducing the proper intermetallics [20]. Birbilis et al. [21,22] reported that the cathodic kinetics of Mg alloys could be significantly reduced by the addition of Arsenic (As) and Germanium (Ge). They attributed this phenomenon to the fact that noble intermetallic compounds, such as Mg<sub>2</sub>Ge, may serve as the ‘sluggish’ sites for HER. A deeper understanding of the cathodic corrosion reaction on Mg

\* Corresponding authors at: University of Michigan - Shanghai Jiao Tong University Joint Institute, Shanghai Jiao Tong University, Shanghai 200240, PR China.  
E-mail addresses: [xqzeng@sjtu.edu.cn](mailto:xqzeng@sjtu.edu.cn) (X. Zeng), [hong.zhu@sjtu.edu.cn](mailto:hong.zhu@sjtu.edu.cn) (H. Zhu).

intermetallics is still missing but of urgent need, which can guide the design of corrosion-resistant Mg alloys.

Since it is difficult to observe the reactions that happen on surfaces and interfaces from the atomic scale by experimental approaches, density functional theory (DFT) simulations can be used as a powerful tool to investigate the corrosion mechanisms. Based on Sabatier principle [23], the high reaction rate for cathodic HER can be achieved when interactions between H adatom and substrate are of moderate strength, while too weak or too strong H-surface binding will suppress the HER so as to reduce the overall corrosion rate of Mg alloys. Meanwhile, from a computational point of view, the binding strength between the H adatom and metal surface could be described by the adsorption energy of H ( $E_{\text{ads}}$ ), which is a good descriptor for the kinetics of cathodic HER. To the best of our knowledge, most of the current theoretical studies related to Mg corrosion focus on HER occurring on the most stable surfaces of Mg matrix, Fe impurity phase or some specific intermetallic compounds [24–26]. Qi et al. [27] utilized DFT computations to calculate  $E_{\text{ads}}$  on Fe impurities in Mg alloys to search for the alloying elements which can effectively impede the cathodic HER on Fe surfaces. Similar studies were also performed to investigate the influence of alloying elements on the cathodic reaction which happened on the most stable surface of Mg matrix [24,28]. However, intermetallics are common existing forms in metals and play a crucial role in the corrosion performance of metal alloys. Up to now, systematic study of corrosion cathodic reaction kinetics on the intermetallics is still lacking. Moreover, the cathodic reactions on the most stable surface may not be enough to represent the overall performance, especially when a few surface terminations have similar surface energies. Chen et al. investigated the Mg anodic and cathodic corrosion reaction separately and they found that different low-index facets show different reaction rates [29,30]. Therefore, it is necessary to consider HER on the possible surface terminations as well as over various active sites. Complex surface configurations and different exposed faces of one Mg intermetallics could increase the computational cost by even two orders of magnitude compared with pure Mg. Thus, to filter the intermetallics with very positive or negative  $E_{\text{ads}}$  to inhibit corrosion cathodic reaction in the vast searching space, it is crucial to develop strategies to accelerate the screening process.

Machine learning (ML) techniques could substantially facilitate the DFT computations [31,32] and active learning [33], also known as the optimal design of experiments, could further decrease the computational cost. The basic idea of active learning is that a surrogate model is trained from a given data set first, and then the model is applied to pick which data should be obtained in the next operation. After the experiment or computation, the obtained data is added to the original data set and then the surrogate model is updated. The process is repeated iteratively so that the predictive performance of the surrogate model is improved continuously. This method has been successfully applied in the development of new catalysts and high entropy alloys with desired properties [34,35]. As for prediction models, Ulissi et al. [36,37] utilized an artificial neural network (ANN) to accurately predict the adsorption energy of specific molecules on bimetallic catalysts, yielding a mean absolute error (MAE) of 0.2 eV from an analysis of approximately 43,000 data entries. Unfortunately, many models currently in use are based on electronic structure information, such as *d*-band center or Bader charge transfer, requiring additional DFT calculations to prepare the ML input features. Therefore, ML models that use easily available input features with high prediction accuracy for  $E_{\text{ads}}$  are strongly desirable to achieve an efficient search over the broad candidate space [38,39].

In this work, we applied the idea of active learning to develop a framework that can accelerate the discovery of corrosion-resistant binary intermetallic compounds for Mg alloys. A total of 275 Mg binary intermetallics are considered and around 100,000 different H adsorption configurations are screened based on the adsorption energy of H ( $E_{\text{ads}}$ ), which is a descriptor of cathodic HER kinetics for corrosion. Eleven classical ML models are trained based on our previously developed datasets [40] and the best-performing model is used for the further

“computation-prediction” loop. The input features of the ML model used in this work are composed of geometric features and chemical features of the H adsorption configuration, which are extracted via Voronoi analysis and do not need additional DFT computations. Finally, we calculated the surface energies of these intermetallics and ranked the ability to hinder the HER of all binary Mg intermetallics based on weighted H adsorption energy to guide future experiments. The features of intermetallic surfaces leading to a weak or strong H binding were also analyzed. It is expected that this framework combining DFT computation and active learning strategy effectively accelerates the discovery of corrosion-resistant binary Mg alloys and inspires the design of other corrosion-resistant metal alloy systems.

## 2. Methods

### 2.1. Computational methods

In this work, all DFT calculations were performed by the projector augmented wave (PAW) [41] method implemented in the Vienna Ab Initio Simulation Package (VASP) [42]. The exchange-correlation functional was described by generalized gradient approximation (GGA) [43] with Perdew-Burke-Ernzerhof approach [44]. When operating high-throughput computation, the cut-off energy of plane wave was set at 480 eV. The convergence criterion of energy was set to  $10^{-5}$  eV/atom. Considering different lattice structures of intermetallics, Gamma-centered k-point grids were automatically generated by pymatgen [45]. To avoid the interaction caused by periodic mirror images, a 15 Å vacuum layer was employed along the Z direction and the surface area of slabs was constructed to be larger than  $50 \text{ \AA}^2$ . 275 Mg binary intermetallics with energy above hull less than 50 meV are collected from Material project and around 100,000 different H adsorption configurations are generated on the low index surfaces of these intermetallics. The adsorption energy of H ( $E_{\text{ads}}$ ) is calculated by

$$E_{\text{ads}} = E_{\text{slab}^*\text{H}} - E_{\text{slab}} - \frac{1}{2}E_{\text{H}_2} \quad (1)$$

where  $E_{\text{slab}^*\text{H}}$ ,  $E_{\text{slab}}$  and  $E_{\text{H}_2}$  are the DFT energies of the slab model with one hydrogen adatom, the bare slab model and one hydrogen molecule, respectively. The optimal or fastest reaction rate of cathodic HER can be achieved when the adsorption free energy of hydrogen atom (denoted as  $\Delta G_{\text{H}^*}$ ) equals to zero [46]. The  $\Delta G_{\text{H}^*}$  can be calculated by

$$\Delta G_{\text{H}^*} = E_{\text{ads}} + \Delta E_{\text{ZPE}} - T\Delta S_{\text{H}} \quad (2)$$

where  $\Delta E_{\text{ZPE}}$  and  $\Delta S_{\text{H}}$  are the difference in zero-point energy and entropy between the adsorbed and the gas phase, respectively.  $\Delta E_{\text{ZPE}} - T\Delta S_{\text{H}}$  is calculated to be 0.19 eV for most of H adsorption on Mg or Mg common intermetallics [47]. Thus, when hydrogen adsorption energy equals to  $-0.19$  eV, the rate of the cathodic corrosion reaction is maximized. The aim of this study is to identify intermetallics with either significantly positive or negative hydrogen adsorption energies.

### 2.2. Machine learning models

Several classical ML models, including linear regression (LR), least absolute shrinkage and selection operator (LASSO), ridge regression (RR), Gaussian processing regression (GPR), support vector regression (SVR), kernel ridge regression (KRR), k-nearest neighbor regression (KNN), gradient boosting regression tree (GBRT), random forest regression (RFR) and Extreme Gradient Boosting (XGBoost) are employed in this work. The whole dataset of  $E_{\text{ads}}$  developed from prior work [40] was divided into 80% (543) training set and 20% (137) test set. The hyperparameters are carefully selected by grid search with five-fold cross validation. The details about the range of the main hyperparameters can be found in Table S1. The accuracy of the models is evaluated by the mean absolute error (MAE). As for the ML

implementation, we use the open-source Python module, Scikit-learn [48].

### 2.3. General design strategy

The iterative feedback loop coupling active learning and DFT computation was applied to predict Mg intermetallic compounds with slow HER, as schematically shown in Fig. 1. The design process is implemented as follows: The features containing geometric and chemical features related to  $E_{\text{ads}}$  are extracted from the initial adsorption configuration in our database based on Voronoi analysis [49]. Then, an ML surrogate model is trained to map the input features and DFT-calculated  $E_{\text{ads}}$ . Subsequently, the possible H adsorption configuration on unexplored Mg binary intermetallic surfaces is enumerated by pymatgen [50] and the above-obtained ML model is applied to predict  $E_{\text{ads}}$  without any ab initio level computation. Finally, for those adsorption configurations with predicted low or high  $E_{\text{ads}}$ , the DFT calculations are performed and newly obtained  $E_{\text{ads}}$  are added to the data set to iteratively improve the performance of ML model.

## 3. Results and discussions

### 3.1. Initial dataset analysis and feature construction

In our previous study, 680  $E_{\text{ads}}$  on the low index surfaces (Miller index up to (111)) of 50 binary Mg intermetallics with high stability and low thermodynamic driving force for galvanic corrosion (or small equilibrium potential difference with respect to Mg matrix) have been calculated [40], whose distribution is shown in Fig. 2a. The majority of the H adsorption energy is located near the optimal hydrogen adsorption energy for fastest HER ( $\sim -0.19$  eV) [30,40], indicating most of these intermetallics will accelerate the cathodic reaction of galvanic corrosion, as discussed in details in methodology part. However, some intermetallics with very slow HER kinetics but relatively larger equilibrium potential differences with respect to pure Mg have been overlooked from our prior strict screening, such as  $\text{Mg}_2\text{Ge}$ . In this work, our aim is to screen the intermetallics with extreme negative or positive  $E_{\text{ads}}$  to suppress the cathodic HER and hence the overall corrosion reaction. Generally speaking, it is hard to train robust ML models with sparse data away from the optimal hydrogen adsorption energy for fastest HER ( $\sim -0.19$  eV). Therefore, the idea of active learning is applied and data towards very negative or positive  $E_{\text{ads}}$  are continuously enriched during active learning. Fig. 2b displays the element distribution of 275 Mg binary intermetallics with energy above hull less than 50

meV considered in this work. Compared with our previous high-throughput screening work [40], both the number of intermetallics and the distribution of elements have increased significantly. Mg-Li, Mg-Al and Mg-Y binary alloy systems contain more intermetallics than other alloy systems.

Feature generation is a crucial step for developing robust ML models. Some criteria are considered in constructing the adsorption configuration-related features: (a) the features should be capable of distinguishing different adsorption sites on the same surface; (b) they must be computationally inexpensive or already available from the database to decrease prediction cost; (c) most importantly, physical intuitive and domain knowledge are needed to ensure the features are highly related with the H adsorption energy. It is expected that the surface atoms near the adsorbate contribute the most to the bonding process. Thus, as shown in Fig. 2c, we first extract the local adsorption environment of H adatom from a slab model based on Voronoi analysis as implemented in Pymatgen. Then, two types of features are generated according to H adatom Voronoi neighbors. The first category is geometry-related features, including Voronoi coordination number of H (CN), the minimum distance between H and surface atom (MD), and so on. The second category describes the elemental properties near the adsorption site. In order to distinguish the contribution of neighbors with different distances from adsorbed H, the weighted chemical features  $\chi$  are calculated by

$$\chi = \sum_{i=1}^N \omega_i \chi_i \quad (3)$$

where  $\chi_i$  is a elemental property of  $i_{\text{th}}$  neighbor,  $N$  is the total coordination number of H,  $\omega_i$  is the normalized weight of the solid angle subtended from the Voronoi polyhedron [51]. Based on the above ideas, a total of 27 features are originally generated. After considering the correlation of features via Pearson correlation coefficient (PCC), 2 features are excluded due to the high linear relationship with other features. The PCC map among all features is supplied in Supporting Information (SI) Figs. S1 and S2 and the details of the features and their abbreviations are supplied in Table S2.

### 3.2. Model selection and active learning iterative loop

Fig. 3a shows the accuracy of eleven ML models for the prediction of H adsorption energy,  $E_{\text{ads}}$ . The errors on the test set are comparable but slightly higher than that on the validation set, indicating these models are well trained. It is obvious that linear regression methods, such as

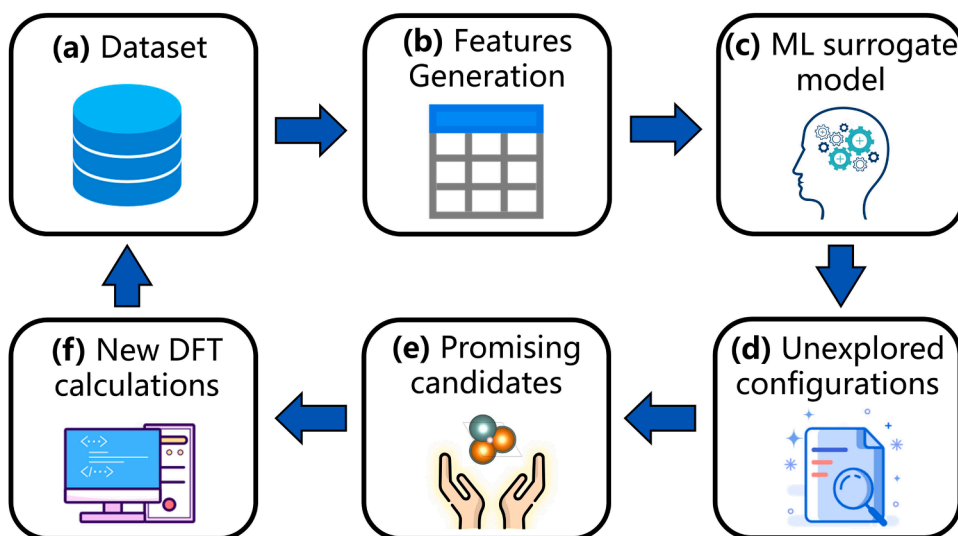


**Fig. 1.** A schematic diagram of active learning design framework to accelerate the discovery of corrosion-resistant binary Mg alloys. (a) The original dataset was collected from our previously developed dataset [40]. (b) Adsorption features, including geometric and chemical features related to  $E_{\text{ads}}$ , were extracted from the initial adsorption configuration based on Voronoi polyhedron. (c) ML surrogate models were trained based on input features. (d) Adsorption configurations of unexplored Mg binary intermetallics were generated by pymatgen. (e) ML models were applied to predict  $E_{\text{ads}}$  and promising candidates with high or low  $E_{\text{ads}}$  were picked. (f) According to prediction, new DFT calculations were performed and the obtained  $E_{\text{ads}}$  were added to the dataset.

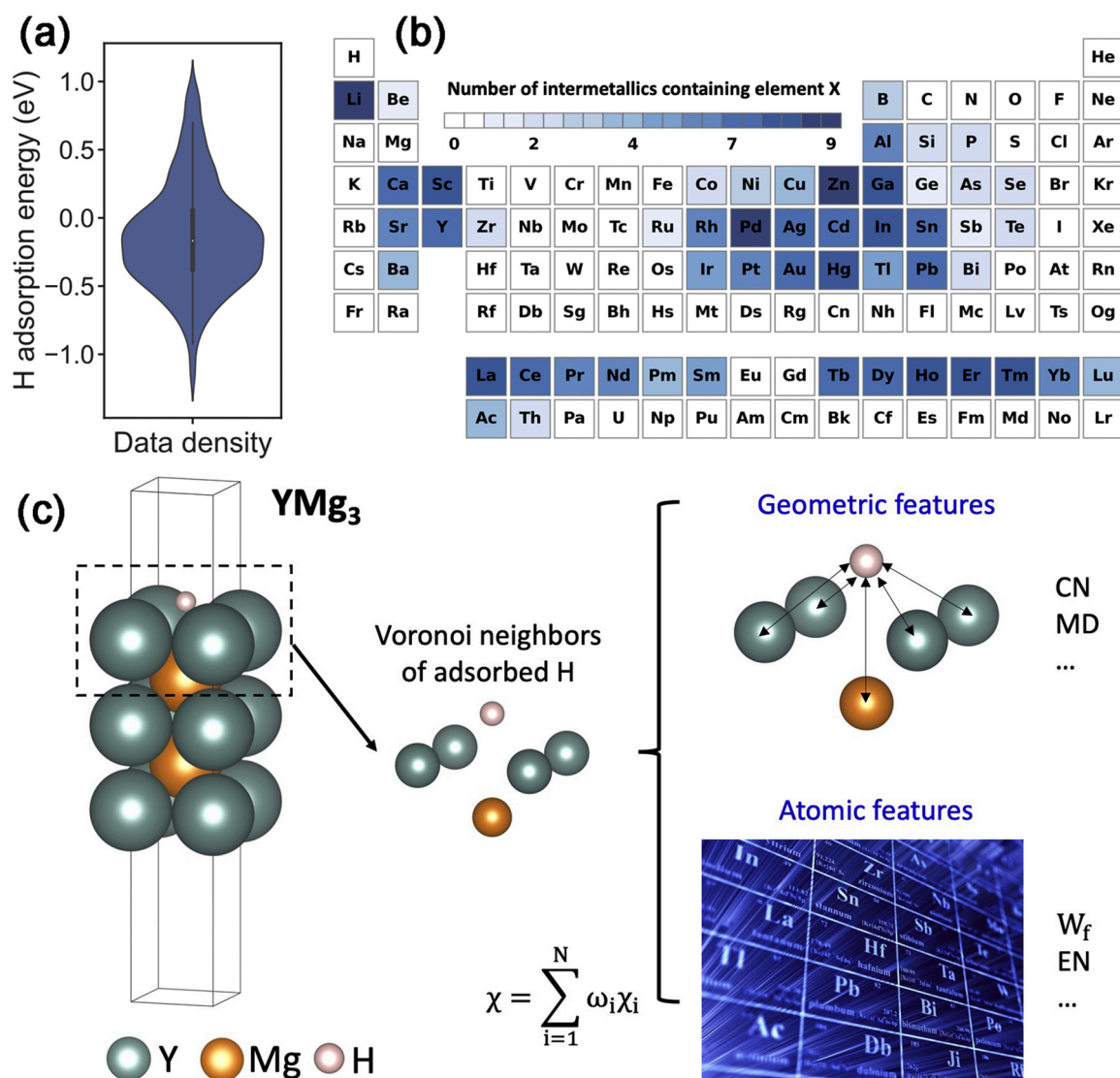


**Fig. 2.** (a) The statistical distribution of the DFT calculated  $E_{\text{ads}}$  from the initial dataset. (b) The number of intermetallics containing element X. The white boxes indicate that no stable or semi-stable intermetallics are found in Material Project database. The darker color of an alloy system represents a greater number of stable or semi-stable intermetallics than other alloy systems. (c) Method to extract the geometric features and chemical features from H adsorption configuration. Take  $\text{YMg}_3$  as an example, the local adsorption environment, namely H adatom and its surrounding Voronoi neighbors, is firstly extracted by Voronoi analysis. Then, geometric features of the local adsorption environment are calculated based on the geometry of Voronoi polyhedron. Chemical features of the local adsorption environment are calculated by the weighted sum of the elemental feature of each Voronoi neighbor. The weights are obtained from the solid angle of the Voronoi polyhedron.

linear regression and LASSO, are significantly worse than other methods. In contrast, the ensemble models, including RFR and XGBoost, outperform other algorithms with the MAE around 0.15 eV since they use a group of base learners trained by different methods or parameters to produce a final prediction. In this paper, XGBoost is chosen to make predictions in the following sections since it performs best among all ML models on the training set. It should be mentioned that the geometric features and chemical features used in this work are extracted from the initial adsorption configurations without any atomic level relaxations. The accuracy of the ML models is expected to improve if the optimized adsorption configurations are employed. However, the reliance on structural relaxation would go against the goal of using easily obtainable features to predict  $E_{\text{ads}}$ .

After selecting XGBoost model, the original dataset is used to train the model and the  $E_{\text{ads}}$  of  $\sim 100,000$  unexplored H adsorption configurations are initially predicted. Only the most negative predicted  $E_{\text{ads}}$  of each surface is selected to represent the corrosion properties of this

surface because some initial H adsorption sites generated by pymatgen may be unreasonable and cause extremely positive  $E_{\text{ads}}$ . During the active learning loops, a system is designed to select iteratively and adaptively which adsorption configurations should be annotated in the next loop instead of asking an expert. The design criterion for this system is picking around 5% new data, namely 40 configurations with extremely negative or positive adsorption energy to perform DFT calculations in each iteration. In addition, to avoid the model only recommending the intermetallics that are already in the training set, in each iteration the system only picked the adsorption configurations which have not been calculated before and the maximum number of the adsorption configurations for the same intermetallics to be simulated in VASP is not more than 2. Then, the DFT calculated adsorption energies and adsorption configurations are added to the training dataset. In this way, the  $E_{\text{ads}}$  data located at relative negative or positive regions are enriched and prediction accuracy for the two regions will also gradually increase. Fig. 3b displays the MAE for each iteration. With more data

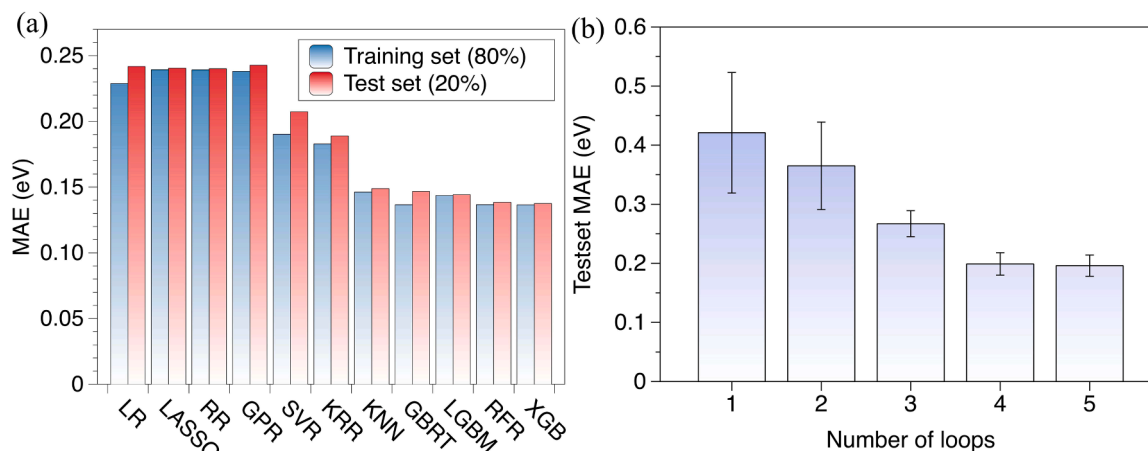


Fig. 3. (a) The average performance of ML models with 25 input features. The dataset is randomly divided into 80% training set and 20% test set. (b) The average MAE of 40 new predicted  $E_{\text{ads}}$  (including 20 strong adsorption cases and 20 weak adsorption cases for each iteration) for 5 active learning iterations.

added to the original dataset, the prediction error and variance of the XGBoost model continuously decrease. It can be observed from Fig. 3b that XGBoost model tends to converge after loop 4 with a slightly higher prediction error than the training set. At iteration 5, the average MAE of XGBoost is at 0.196 eV. After weighting the model prediction accuracy against the computational cost, we decided to stop the iteration at loop 5. The error of our model for  $E_{\text{ads}}$  prediction is comparable to the errors of other machine learning or deep learning methods currently available [37,52–54]. Although utilizing more data and employing intricate deep learning techniques may lead to a partial reduction in the prediction error of H adsorption energy, our method stands out due to its remarkable efficiency and practicality, as it requires significantly less data and does not involve any surface relaxation or H adsorption calculations. This advantage enables its widespread applicability across various domains.

### 3.3. Feature importance analysis

XGBoost not only can predict the adsorption energy of H for an initial adsorption configuration, but also provide some information about the importance of the input features. Fig. 4a shows the Gini importance [55] of the features ranked by their influence on the  $E_{\text{ads}}$ . It should be noted that the utilized features in this work are the weighted average elemental properties of Voronoi neighbors and the geometric characteristics of adsorption configurations. For example, the work function (WF) in Fig. 4a indicates the weighted average work function of all Voronoi neighbors and the weights are from the solid angle of the Voronoi polyhedron. The features based on Voronoi analysis can well distinguish different adsorption sites on the same surface and help to uncover the comprehensive effect of the surface geometry and chemistry on H adsorption. It can be concluded that the weighted work function (WF) of Voronoi neighbors for H adatom is the most influential feature

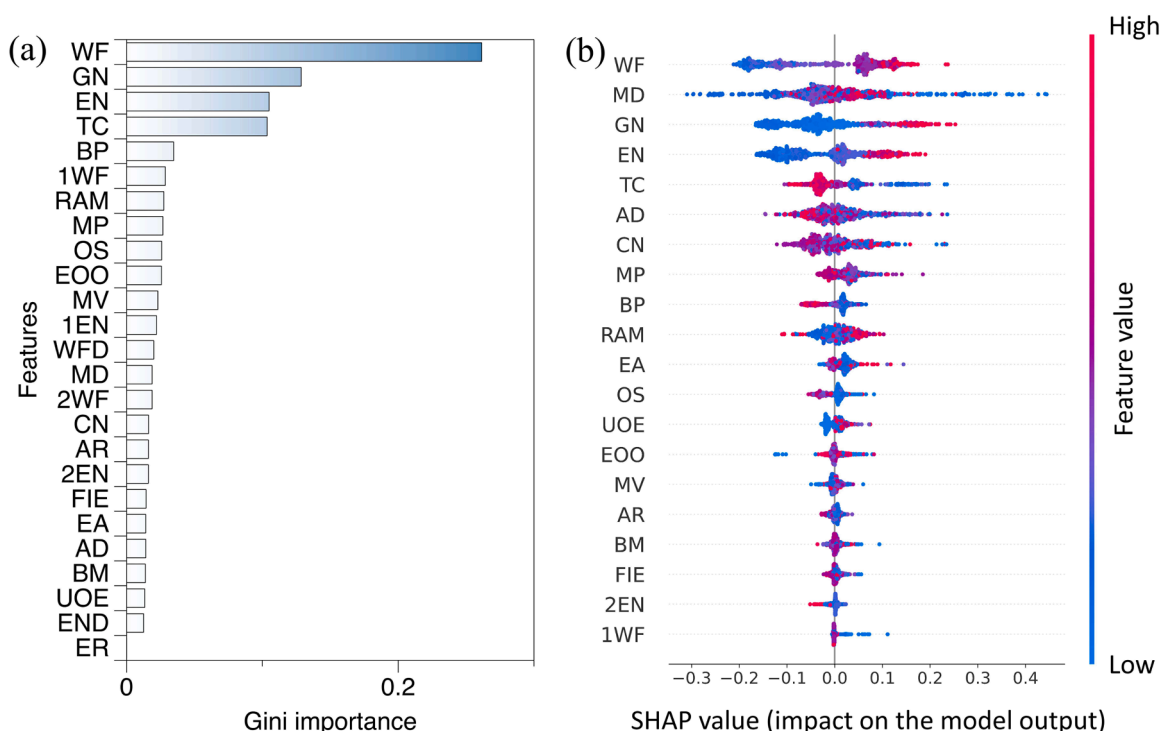


Fig. 4. (a) The feature importance obtained from XGBoost based on Gini importance. (b) Feature importance obtained by SHAP (Shapley Additive Explanations).

to predict  $E_{\text{ads}}$  with the Gini importance of 0.26. Peng et al. [56] also found that the work function of the surface is a good parameter to predict adsorption energy on transition metals, but their model cannot distinguish the various adsorption sites for the same surface, which are associated with different  $E_{\text{ads}}$ . The second and third most important features are weighted average group number (GN) and electronegativity (EN) of the Voronoi neighbors for H adatom. In fact, group number and electronegativity are correlated with each other and they are all positively related to the work function. These three chemical properties can evaluate the ability to bind electrons for an atom so as to influence the bonding strength with H.

To understand the mapping relationship between the input features and H adsorption energy, Shapley Additive Explanations (SHAP) [57] is applied to interpret the predictions of the ML models. Compared with the importance obtained from XGBoost, SHAP can give a more visual impression of how the features influence  $E_{\text{ads}}$ . The color of the single point in SHAP plot indicates the feature's value and the features are also ranked by their importance. As shown in Fig. 4b, weighted average work function of H Voronoi neighbors is also considered as the most important feature in forecasting the  $E_{\text{ads}}$ . With the increase of the weighted work function for H Voronoi neighbors (data points color from blue to red), the H adsorption energy will also increase, indicating that the H adsorption becomes less stable. Interestingly, from a material science point of view, similar conclusion can also be drawn. Work function, as the minimum energy required to transport an electron at Fermi level to field-free region external to the surface [58], is a crucial physical parameter to determine the stability of the materials. In this regard, the surfaces with larger work function are usually conjugated with high stability. Moreover, higher stability will transfer fewer electrons to hydrogen atom and therefore the bonding with H atom will be weaker, leading to higher  $E_{\text{ads}}$ . Similar trends can be observed on weighted average group number (GN) and electronegativity (EN) of the H Voronoi neighbors. Higher values of these two features correspond to higher  $E_{\text{ads}}$ .

### 3.4. Bader charge analysis

To further understand the varied binding strengths of H with different intermetallic surfaces, the electronic structure analysis of some representative surfaces has been performed. Here, two strong adsorption surfaces ( $\text{Ho}_5\text{Mg}$  and  $\text{YMg}$ ) and two weak adsorption surfaces ( $\text{MgSn}_3$  and  $\text{MgTl}$ ) are picked to perform Bader charge and density of states (DOS) analyses. The positive and negative signs in the left panel of Fig. 5

represent the atom's valence state after H adsorption. It is obvious that the electrons transferred to the H adatoms on the strong adsorption surface ( $0.71e^- \sim 0.83e^-$ ) are greater than those on the weak adsorption surface ( $0.37e^- \sim 0.39e^-$ ). We notice that the Voronoi neighbors of the strong adsorption surfaces (more negative  $E_{\text{ads}}$ ) are usually with small electronegativity, which means the electrons on the surfaces are more likely to be free electrons and participate in the bonding process with H adatoms. In contrast, the Voronoi neighbors of the weak adsorption surfaces (more positive  $E_{\text{ads}}$ ) possess a large electronegativity, in competition with adsorbed H in terms of getting electrons. The DOS of H in Fig. S3 further indicates that the DOS of H adatom on strong adsorption surface is sharp and much lower than the Fermi level, indicating there is a strong bonding between H adatom and surface. However, the DOS of adsorbed H on weak adsorption surface is flat and near the Fermi level. To further understand the relationship between charge transferred to H adatom and weighted average properties of Voronoi neighbors such as electronegativity as well as work function, which are the most important factors obtained from feature importance analysis. The right panels of Fig. 5 display the properties of the strong and weak adsorption surface by radar charts. The values are normalized between 0 and 1 and detailed values are supplied in Table S3. It is obvious that the H adatom Voronoi neighbors with greater weighted average electronegativity and work function contribute to less charge transferring to H adatoms, consistent with our finding in Section 3.3. This result suggests that ML can provide insight into chemical and physical principles governing the adsorption process. In addition, compared with directly using the chemical properties of the second element in Mg alloys as machine learning input, the features extracted by Voronoi analysis can effectively distinguish different adsorption sites on the same surface.

### 3.5. Searching promising binary Mg intermetallics to inhibit galvanic corrosion

After predicting the  $E_{\text{ads}}$  on different binary Mg intermetallic surfaces via XGBoost, it is necessary to evaluate the overall ability to hinder Mg corrosion cathodic reaction based on the thermodynamic stability of exposure surfaces. Some surfaces which can strongly impede the HER, however, may not be thermodynamically stable, which can cause the discrepancy between computational results and experimental observations. The exposure surfaces of 275 intermetallics are cleaved mainly symmetrically up to maximum Miller index of (111) using the python package pymatgen [45]. The surface energies are then calculated under

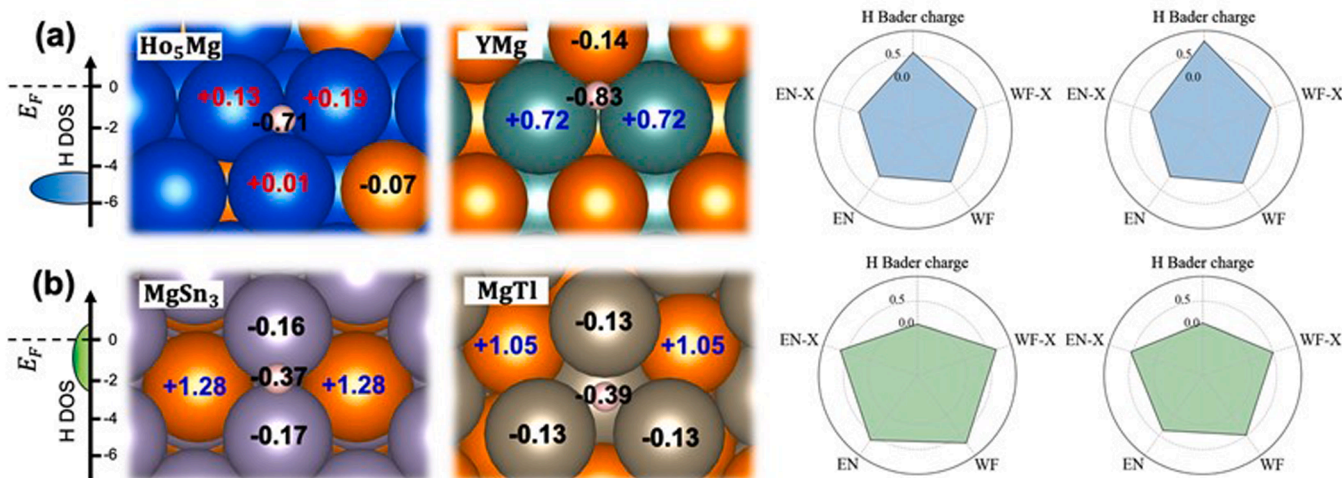


Fig. 5. Bader charge analysis and surface properties of (a) strong and (b) weak H adsorption surfaces. The left subfigs. are the schematic draw of density states of adsorbed H. The EN-X and WF-X on the right panel are the electronegativity and work function of the second element in binary Mg intermetallics. EN and WF are the weighted average electronegativity and work function of H adatom Voronoi neighbors. All the properties are normalized between 0 and 1. The details of the surface properties and normalized interval are supplied in Table S3.

the Mg rich condition and the detailed method can be found in our previous studies [59,60]. For those binary intermetallics which cannot have symmetric exposure surfaces, we calculated the average surface energy. Finally, we obtained 5524 surface energies in total, and these data are of great significance in analyzing the surface stability as well as the corrosion property of binary Mg alloys. By taking  $Mg_2Ge$  as an example, Fig. 6a–c illustrate how to calculate  $E_{wads}$  for a certain intermetallic phase. Fig. 6a and 6b show the unit cell of  $Mg_2Ge$  and the Wulff shape of  $Mg_2Ge$  constructed by the low-index surface energy. The box plot in Fig. 6c displays the distribution of the most stable predicted H adsorption energy among various exposure surfaces of  $Mg_2Ge$ . The weighted H adsorption energy  $E_{wads}$ , denoted as the black star, is calculated by

$$E_{wads} = \sum_{i=1}^N x_i E_{ads} \quad (4)$$

where  $N$  is the number of the exposure surfaces in Wulff shape,  $x_i$  is the normalized surface area fraction of  $i_{th}$  surface,  $E_{ads}$  is the most stable predicted H adsorption energy of the  $i_{th}$  surface. Since  $E_{wads}$  considers the adsorption properties of different surfaces for an intermetallic compound, it is believed to be a better indicator to evaluate the ability to

suppress the cathodic reaction.

Fig. 6d and 6e display the ranking of Mg intermetallics based on the weighted adsorption energy (denoted as the black star), which represents their ability to suppress the corrosion cathodic reaction for the strong and weak H adsorption. To validate the calculations, we conducted a comparison between the cathodic exchange current density extrapolated from experimental polarization curves and the ones determined from our simulations according to a kinetic model proposed by Nørskov [46]. A strong linear relationship was observed between the extrapolated and calculated exchange current density, indicating our computational data offer significant guidance for experimental work. The specific details can be found in Fig. S4. From the results depicted in Fig. 6d, the intermetallics with strong H adsorption ability are mainly concentrated in lanthanide (La) systems. Previously, the reason why rare earth elements can improve the corrosion performance of Mg alloys is mainly attributed to refining the microstructure and the formation of dense oxide film [5,61]. In this paper, we believe that some intermetallics of Mg-La binary system can also effectively inhibit HER and thus reduce the corrosion rate of Mg alloys. In addition, it can be observed from Fig. 6d that the elements for the strong H adsorption intermetallics are usually with relatively small electronegativity, e.g. Y (1.22), Dy (1.22) and La (1.10), compared with H (2.20). The large

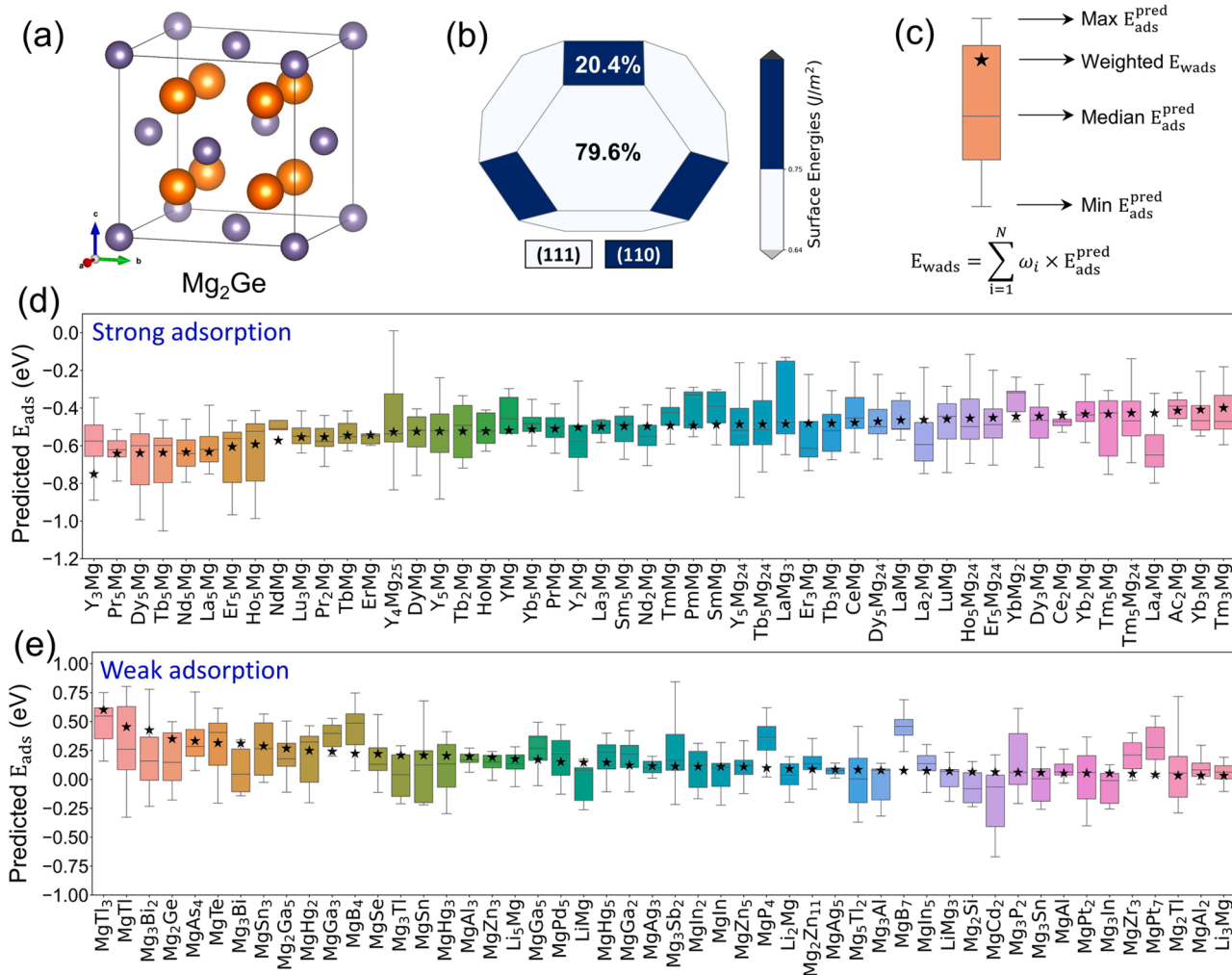


**Fig. 6.** The screened binary Mg intermetallics that can hinder the cathodic HER,  $Mg_2Ge$  is used as an example to illustrate how to measure the ability of an intermetallic compound to inhibit the cathodic corrosion reaction of Mg alloys. (a) The unit cell of  $Mg_2Ge$  where the orange atom is Mg and purple atom is Ge. (b) The constructed Wulff shape of  $Mg_2Ge$  crystal. The surface energy is in the unit of  $J/m^2$ . The percentage represents the proportion of each crystal plane. (c) XGBoost predicted adsorption energy range of an intermetallic with different surfaces and different adsorption sites. The intermetallics are ranked by weighted adsorption energy ( $E_{wads}$ ), shown as black stars, which is calculated by the weighted average of the most negative ML predicted  $E_{ads}$  on each surface and the corresponding surface ratio. (d) Top 50 intermetallics with strong H adsorption. (e) Top 50 intermetallics with weak H adsorption.

difference in the ability of bonding electrons leads to more electrons accumulating around the H during the adsorption process. Similarly, we can conclude that most of the second elements in weak H adsorption intermetallics have high electronegativity. The electronegativities of elements in the top three weak adsorption intermetallics are Tl (1.80), Bi (1.90) and Ge (2.01). Birbilis et al. considered that Mg<sub>2</sub>Ge could effectively hinder the HER by observing the cathodic part of polarization curves for pure Mg and Mg-Mg<sub>2</sub>Ge alloy systems [22]. In our study, the Mg<sub>2</sub>Ge is also recommended as the intermetallics with weak H adsorption ability based on the ranking of the weighted average H adsorption energy in our results.

As we have discussed above, the weighted H adsorption energy ( $E_{\text{wads}}$ ) can be applied to describe the kinetics of corrosion cathodic reactions on Mg intermetallic compounds. Potentially, for an energetically favored surface termination, such a screening process could be further simplified, where the weighted electronegativity or work function of the H adatom Voronoi neighbors can be directly applied to evaluate whether there will be a sluggish HER, which may be applied to the design of other metal alloy systems, e.g. ternary Mg alloys with more complex intermetallic compounds or even other metal alloy systems. Further work regarding the effects of alloying elements on the corrosion anodic reaction for Mg alloys is also in need to comprehensively investigate the influence of doping elements on the total corrosion reaction of the Mg alloys.

#### 4. Conclusion

The present work was conducted to discover the corrosion-resistant binary Mg alloys with intermetallic compounds showing sluggish HER by means of density functional theory computation and active learning. Active learning has been shown to significantly reduce the number of training samples while maintaining the prediction accuracy (MAE of 0.196 eV) of the H adsorption energy with easily captured features. In order to understand the reasons for the different adsorption capacities of hydrogen atoms on the different surfaces, several representative surfaces are picked to perform Bader charge and density of states (DOS) analysis. These results indicate that the electrons transferred to the H atoms on the strong adsorption surface are greater than those on the weak adsorption surface. Finally, the ability to impede HER of intermetallics is ranked based on surface stability and predicted H adsorption energy, which provides insights for further experiments. Mg intermetallics like Y<sub>3</sub>Mg and MgTl<sub>3</sub> and Mg<sub>2</sub>Ge etc. are considered promising candidates to decrease the corrosion cathodic reaction rate. This study not only realizes the exploration of large-scale unknown space with a small amount of training data through the idea of active learning, but also provides promising intermetallics which can inhibit the galvanic corrosion of Mg alloys from the perspective of cathodic reaction, which could drive for corrosion-resistant Mg alloy design.

#### Data availability

The full data set (1.33 GB), including around 100k different H adsorption structures of the Mg intermetallic phases and the corresponding predicted H adsorption energy, can be downloaded from Google Drive, the link is: <https://drive.google.com/file/d/12ixED-fre9fCH5Bzj6DQJ7tNa1DR2zNsL/view>.

#### Code availability

The source code and scripts of this paper are publicly available at <https://gitlab.com/iamds/Mg-Corrosion-DFT-data>.

#### Declaration of Competing Interest

The authors declare that they have no known competing financial interests or personal relationships that could have appeared to influence

the work reported in this paper.

#### Acknowledgments

The research was financially supported by the National Key R&D Program (No. No. 2021YFB3501002) supported by the Ministry of Science and Technology of China, National Natural Science Foundation of China (No. 51825101, 52127801). First-principles calculations were carried out on the  $\pi$  2.0 cluster supported by the Center for High Performance Computing at Shanghai Jiao Tong University.

#### Supplementary materials

Supplementary material associated with this article can be found, in the online version, at [doi:10.1016/j.actamat.2023.119063](https://doi.org/10.1016/j.actamat.2023.119063).

#### References

- [1] M. Esmaily, J.E. Svensson, S. Fajardo, N. Birbilis, G.S. Frankel, S. Virtanen, R. Arrabal, S. Thomas, L.G. Johansson, Fundamentals and advances in magnesium alloy corrosion, *Prog. Mater. Sci.* 89 (2017) 92–193, <https://doi.org/10.1016/j.pmatsci.2017.04.011>.
- [2] H.R. Bakhsheshi-Rad, E. Hamzah, A. Fereidouni-Lotfabad, M. Daroonparvar, M.A. M. Yajid, M. Mezbahul-Islam, M. Kasiri-Asgarani, M. Medraj, Microstructure and bio-corrosion behavior of Mg-Zn and Mg-Zn-Ca alloys for biomedical applications: microstructure and bio-corrosion behavior of Mg-Zn and Mg-Zn-Ca alloys, *Mater. Corros.* 65 (2014) 1178–1187, <https://doi.org/10.1002/maco.201307588>.
- [3] Y. Zhang, D. Tao, F. Xu, T. Li, A low-cost and high-performance rechargeable magnesium battery based on povidone iodine cathode, *Chem. Eng. J.* 427 (2022), 131592, <https://doi.org/10.1016/j.cej.2021.131592>.
- [4] S.R. Golroudbary, I. Makarava, E. Repo, A. Kraslawski, P. Luukka, Magnesium life cycle in automotive industry, *Procedia CIRP* 105 (2022) 589–594, <https://doi.org/10.1016/j.procir.2022.02.098>.
- [5] K. Gusieva, C.H.J. Davies, J.R. Scully, N. Birbilis, Corrosion of magnesium alloys: the role of alloying, *Int. Mater. Rev.* 60 (2015) 169–194, <https://doi.org/10.1179/1743280414Y.00000000046>.
- [6] E. McCafferty, *Introduction to Corrosion Science*, Springer, New York, New York, NY, 2010, <https://doi.org/10.1007/978-1-4419-0455-3>.
- [7] A.D. Südholz, N.T. Kirkland, R.G. Buchheit, N. Birbilis, Electrochemical properties of intermetallic phases and common impurity elements in magnesium alloys, *Electrochem. Solid-State Lett.* 14 (2010) C5, <https://doi.org/10.1149/1.3523229>.
- [8] C. Wang, W. Xu, D. Höche, M.L. Zheludkevich, S.V. Lamaka, Exploring the contribution of oxygen reduction reaction to Mg corrosion by modeling assisted local analysis, *J. Magnes. Alloy.* 11 (2023) 100–109, <https://doi.org/10.1016/j.jma.2022.09.031>.
- [9] E.L. Silva, S.V. Lamaka, D. Mei, M.L. Zheludkevich, The reduction of dissolved oxygen during magnesium corrosion, *ChemistryOpen* 7 (2018) 664–668, <https://doi.org/10.1002/open.201800076>.
- [10] L. Wang, T. Shinohara, B.P. Zhang, Influence of deaerated condition on the corrosion behavior of AZ31 magnesium alloy in dilute NaCl solutions, *Mater. Trans.* 50 (2009) 2563–2569, <https://doi.org/10.2320/matertrans.M2009191>.
- [11] D. Höche, Simulation of corrosion product deposit layer growth on bare magnesium galvanically coupled to aluminum, *J. Electrochem. Soc.* 162 (2015) C1–C11, <https://doi.org/10.1149/2.0071501jes>.
- [12] M. Strebl, M. Bruns, S. Virtanen, Editors' Choice-respirometric *in situ* methods for real-time monitoring of corrosion rates: Part I. Atmospheric corrosion, *J. Electrochem. Soc.* 167 (2020), 021510, <https://doi.org/10.1149/1945-7111/ab6c61>.
- [13] M.G. Strebl, M.P. Bruns, G. Schulze, S. Virtanen, Respirometric *in situ* methods for real-time monitoring of corrosion rates: Part II. Immersion, *J. Electrochem. Soc.* 168 (2021), 011502, <https://doi.org/10.1149/1945-7111/abdb4a>.
- [14] C. Feiler, D. Mei, B. Vaghefinazari, T. Würger, R.H. Meißner, B.J.C. Luthringer-Feyerabend, D.A. Winkler, M.L. Zheludkevich, S.V. Lamaka, In silico screening of modulators of magnesium dissolution, *Corros. Sci.* 163 (2020), 108245, <https://doi.org/10.1016/j.corsci.2019.108245>.
- [15] A. Gungor, A. Incesu, Effects of alloying elements and thermomechanical process on the mechanical and corrosion properties of biodegradable Mg alloys, *J. Magnes. Alloy.* 9 (2021) 241–253, <https://doi.org/10.1016/j.jma.2020.09.009>.
- [16] J. Xie, J. Zhang, Z. You, S. Liu, K. Guan, R. Wu, J. Wang, J. Feng, Towards developing Mg alloys with simultaneously improved strength and corrosion resistance via RE alloying, *J. Magnes. Alloy.* 9 (2021) 41–56, <https://doi.org/10.1016/j.jma.2020.08.016>.
- [17] T. Würger, D. Mei, B. Vaghefinazari, D.A. Winkler, S.V. Lamaka, M. L. Zheludkevich, R.H. Meißner, C. Feiler, Exploring structure-property relationships in magnesium dissolution modulators, *NPJ Mater. Degrad.* 5 (2021) 1–10, <https://doi.org/10.1038/s41529-020-00148-z>.
- [18] R.B. Heimann, Magnesium alloys for biomedical application: advanced corrosion control through surface coating, *Surf. Coat. Technol.* 405 (2021), 126521, <https://doi.org/10.1016/j.surfcoat.2020.126521>.
- [19] F. Czerwinski, Magnesium alloys: properties in solid and liquid states, *BoD – Books on Demand*, 2014.

- [20] Y. Ding, C. Wen, P. Hodgson, Y. Li, Effects of alloying elements on the corrosion behavior and biocompatibility of biodegradable magnesium alloys: a review, *J. Mater. Chem. B* 2 (2014) 1912–1933, <https://doi.org/10.1039/C3TB21746A>.
- [21] N. Birbilis, G. Williams, K. Gusieva, A. Samaniego, M.A. Gibson, H.N. McMurray, Poisoning the corrosion of magnesium, *Electrochem. Commun.* 34 (2013) 295–298, <https://doi.org/10.1016/j.elecom.2013.07.021>.
- [22] R.L. Liu, M.F. Hurlley, A. Kvrnan, G. Williams, J.R. Scully, N. Birbilis, Controlling the corrosion and cathodic activation of magnesium via microalloying additions of Ge, *Sci. Rep.* 6 (2016) 28747, <https://doi.org/10.1038/srep28747>.
- [23] A.J. Medford, A. Vojvodic, J.S. Hummelshøj, J. Voss, F. Abild-Pedersen, F. Studt, T. Bligaard, A. Nilsson, J.K. Nørskov, From the Sabatier principle to a predictive theory of transition-metal heterogeneous catalysis, *J. Catal.* 328 (2015) 36–42, <https://doi.org/10.1016/j.jcat.2014.12.033>.
- [24] K.R. Limmer, K.S. Williams, J.P. Labukas, J.W. Andzelm, First principles modeling of cathodic reaction thermodynamics in dilute magnesium alloys, *Corrosion* 73 (2017) 506–517, <https://doi.org/10.5006/2274>.
- [25] K.S. Williams, J.P. Labukas, V. Rodriguez-Santiago, J.W. Andzelm, First principles modeling of water dissociation on Mg(0001) and development of a Mg surface Pourbaix diagram, *Corrosion* 71 (2015) 209–223, <https://doi.org/10.5006/1322>.
- [26] K.S. Williams, Modeling reaction pathways for hydrogen evolution and water dissociation on magnesium, *Electrochim. Acta* 210 (2016) 261–270, <https://doi.org/10.1016/j.electacta.2016.04.128>.
- [27] M. Zhang, L.G. Hector, Y. Guo, M. Liu, L. Qi, First-principles search for alloying elements that increase corrosion resistance of Mg with second-phase particles of transition metal impurities, *Comput. Mater. Sci.* 165 (2019) 154–166, <https://doi.org/10.1016/j.commatsci.2019.04.018>.
- [28] A. Sumer, S. Chaudhuri, A first principles investigation of corrosion chemistry of common elemental impurities in Mg-Al alloys, *Corrosion* 73 (2017) 596–604, <https://doi.org/10.5006/2392>.
- [29] H. Ma, X.Q. Chen, R. Li, S. Wang, J. Dong, W. Ke, First-principles modeling of anisotropic anodic dissolution of metals and alloys in corrosive environments, *Acta Mater.* 130 (2017) 137–146, <https://doi.org/10.1016/j.actamat.2017.03.027>.
- [30] H. Ma, L. Wu, C. Liu, M. Liu, C. Wang, D. Li, X.Q. Chen, J. Dong, W. Ke, First-principles modeling of the hydrogen evolution reaction and its application in electrochemical corrosion of Mg, *Acta Mater.* 183 (2020) 377–389, <https://doi.org/10.1016/j.actamat.2019.11.025>.
- [31] Z.W. Ulissi, A.J. Medford, T. Bligaard, J.K. Nørskov, To address surface reaction network complexity using scaling relations machine learning and DFT calculations, *Nat. Commun.* 8 (2017) 14621, <https://doi.org/10.1038/ncomms14621>.
- [32] P. Schindler, E.R. Antoniuk, G. Cheon, Y. Zhu, E.J. Reed, Discovery of materials with extreme work functions by high-throughput density functional theory and machine learning, *ArXiv201110905 Cond-Mat Physicsphysics*. (2020). <http://arxiv.org/abs/2011.10905> (accessed September 21, 2021).
- [33] L. Bassman, P. Rajak, R.K. Kalia, A. Nakano, F. Sha, J. Sun, D.J. Singh, M. Aykol, P. Huck, K. Persson, P. Vashista, Active learning for accelerated design of layered materials, *NPJ Comput. Mater.* 4 (2018) 74, <https://doi.org/10.1038/s41524-018-0129-0>.
- [34] M. Zhong, K. Tran, Y. Min, C. Wang, Z. Wang, C.T. Dinh, P. De Luna, Z. Yu, A. S. Rasouli, P. Brodersen, S. Sun, O. Voznyy, C.S. Tan, M. Askerka, F. Che, M. Liu, A. Seifitokaldani, Y. Pang, S.C. Lo, A. Ip, Z. Ulissi, E.H. Sargent, Accelerated discovery of CO<sub>2</sub> electrocatalysts using active machine learning, *Nature* 581 (2020) 178–183, <https://doi.org/10.1038/s41586-020-2242-8>.
- [35] C. Wen, Y. Zhang, C. Wang, D. Xue, Y. Bai, S. Antonov, L. Dai, T. Lookman, Y. Su, Machine learning assisted design of high entropy alloys with desired property, *Acta Mater.* 170 (2019) 109–117, <https://doi.org/10.1016/j.actamat.2019.03.010>.
- [36] Z. Li, S. Wang, W.S. Chin, L.E. Achenie, H. Xin, High-throughput screening of bimetallic catalysts enabled by machine learning, *J. Mater. Chem. A* 5 (2017) 24131–24138, <https://doi.org/10.1039/C7TA01812F>.
- [37] K. Tran, Z.W. Ulissi, Active learning across intermetallics to guide discovery of electrocatalysts for CO<sub>2</sub> reduction and H<sub>2</sub> evolution, *Nat. Catal.* 1 (2018) 696–703, <https://doi.org/10.1038/s41929-018-0142-1>.
- [38] Y. Li, B. Xiao, Y. Tang, F. Liu, X. Wang, F. Yan, Y. Liu, Center-environment feature model for machine learning study of spinel oxides based on first-principles computations, *J. Phys. Chem. C* 124 (2020) 28458–28468, <https://doi.org/10.1021/acs.jpcc.0c06958>.
- [39] X. Wang, B. Xiao, Y. Li, Y. Tang, F. Liu, J. Chen, Y. Liu, First-principles based machine learning study of oxygen evolution reactions of perovskite oxides using a surface center-environment feature model, *Appl. Surf. Sci.* 531 (2020), 147323, <https://doi.org/10.1016/j.apsusc.2020.147323>.
- [40] Y. Wang, T. Xie, Q. Tang, M. Wang, T. Ying, H. Zhu, X. Zeng, High-throughput calculations combining machine learning to investigate the corrosion properties of binary Mg alloys, *J. Magnes. Alloy.* (2022), S221395672200010X, <https://doi.org/10.1016/j.jma.2021.12.007>.
- [41] P.E. Blöchl, Projector augmented-wave method, *Phys. Rev. B* 50 (1994) 17953–17979, <https://doi.org/10.1103/PhysRevB.50.17953>.
- [42] G. Kresse, J. Furthmüller, Efficient iterative schemes for *ab initio* total-energy calculations using a plane-wave basis set, *Phys. Rev. B* 54 (1996) 11169–11186, <https://doi.org/10.1103/PhysRevB.54.11169>.
- [43] J.P. Perdew, W. Yue, Accurate and simple density functional for the electronic exchange energy: generalized gradient approximation, *Phys. Rev. B* 33 (1986) 8800–8802, <https://doi.org/10.1103/PhysRevB.33.8800>.
- [44] J.P. Perdew, K. Burke, M. Ernzerhof, Generalized gradient approximation made simple, *Phys. Rev. Lett.* 77 (1996) 3865–3868, <https://doi.org/10.1103/PhysRevLett.77.3865>.
- [45] S.P. Ong, W.D. Richards, A. Jain, G. Hautier, M. Kocher, S. Cholia, D. Gunter, V. L. Chevrier, K.A. Persson, G. Ceder, Python materials genomics (pymatgen): a robust, open-source python library for materials analysis, *Comput. Mater. Sci.* 68 (2013) 314–319, <https://doi.org/10.1016/j.commatsci.2012.10.028>.
- [46] J.K. Nørskov, T. Bligaard, A. Logadottir, J.R. Kitchin, J.G. Chen, S. Pandalov, U. Stimming, Trends in the exchange current for hydrogen evolution, *J. Electrochem. Soc.* 152 (2005) J23, <https://doi.org/10.1149/1.1856988>.
- [47] Y. Wang, T. Xie, Q. Tang, M. Wang, T. Ying, H. Zhu, X. Zeng, High-throughput calculations combining machine learning to investigate the corrosion properties of binary Mg alloys, *J. Magnes. Alloy.* (2022), <https://doi.org/10.1016/j.jma.2021.12.007>.
- [48] F. Pedregosa, G. Varoquaux, A. Gramfort, V. Michel, B. Thirion, O. Grisel, M. Blondel, P. Prettenhofer, R. Weiss, V. Dubourg, J. Vanderplas, A. Passos, D. Cournapeau, Scikit-learn: machine learning in python, *J. Mach. Learn. Res.* 12 (2011) 2825–2830.
- [49] H. Pan, A.M. Ganose, M. Horton, M. Aykol, K.A. Persson, N.E.R. Zimmermann, A. Jain, Benchmarking coordination number prediction algorithms on inorganic crystal structures, *Inorg. Chem.* 60 (2021) 1590–1603, <https://doi.org/10.1021/acs.inorgchem.0c02996>.
- [50] J.H. Montoya, K.A. Persson, A high-throughput framework for determining adsorption energies on solid surfaces, *NPJ Comput. Mater.* 3 (2017) 14, <https://doi.org/10.1038/s41524-017-0017-z>.
- [51] V.A. Blatov, Voronoi–dirichlet polyhedra in crystal chemistry: theory and applications, *Crystallogr. Rev.* 10 (2004) 249–318, <https://doi.org/10.1080/08893110412331323170>.
- [52] S. Back, J. Yoon, N. Tian, W. Zhong, K. Tran, Z.W. Ulissi, Convolutional neural network of atomic surface structures to predict binding energies for high-throughput screening of catalysts, *J. Phys. Chem. Lett.* 10 (2019) 4401–4408, <https://doi.org/10.1021/acs.jpcclett.9b01428>.
- [53] B.M. Abraham, P. Sinha, P. Halder, J.K. Singh, Fusing a machine learning strategy with density functional theory to hasten the discovery of 2D MXene-based catalysts for hydrogen generation, *J. Mater. Chem. A* 11 (2023) 8091–8100, <https://doi.org/10.1039/D3TA00344B>.
- [54] X. Li, B. Li, Z. Yang, Z. Chen, W. Gao, Q. Jiang, A transferable machine-learning scheme from pure metals to alloys for predicting adsorption energies, *J. Mater. Chem. A* 10 (2022) 872–880, <https://doi.org/10.1039/D1TA09184K>.
- [55] B.H. Menze, B.M. Kelm, R. Masuch, U. Himmelreich, P. Bachert, W. Petrich, F. A. Hamprecht, A comparison of random forest and its Gini importance with standard chemometric methods for the feature selection and classification of spectral data, *BMC Bioinform.* 10 (2009) 213, <https://doi.org/10.1186/1471-2105-10-213>.
- [56] X. Shen, Y. Pan, B. Liu, J. Yang, J. Zeng, Z. Peng, More accurate depiction of adsorption energy on transition metals using work function as one additional descriptor, *Phys. Chem. Chem. Phys.* 19 (2017) 12628–12632, <https://doi.org/10.1039/C7CP01817G>.
- [57] S.M. Lundberg, S.I. Lee, A unified approach to interpreting model predictions, in: *Unified Approach Interpret. Model Predict.*, 2017: pp. 4765–4774.
- [58] S. Halas, T. Durakiewicz, Work functions of elements expressed in terms of the Fermi energy and the density of free electrons, *J. Phys. Condens. Matter* 10 (1998) 10815–10826, <https://doi.org/10.1088/0953-8984/10/48/005>.
- [59] Y. Wang, T. Xie, Z. Luo, H. Zhu, X. Zeng, First-principles study of water decomposition and hydrogen evolution on MgZn<sub>2</sub> Laves phase, *Comput. Mater. Sci.* 196 (2021), 110532, <https://doi.org/10.1016/j.commatsci.2021.110532>.
- [60] A.F. Kohan, G. Ceder, D. Morgan, C.G. Van de Walle, First-principles study of native point defects in ZnO, *Phys. Rev. B* 61 (2000) 15019–15027, <https://doi.org/10.1103/PhysRevB.61.15019>.
- [61] P. Zhao, T. Xie, X. Xu, H. Zhu, F. Cao, T. Ying, X. Zeng, Designing high corrosion resistant peritectic magnesium alloys via Sc and Y addition, *Metall. Mater. Trans. A* 51 (2020) 2509–2522, <https://doi.org/10.1007/s11661-020-05693-5>.